Effect of doping Fe^{3+} and Cu^{2+} on the microstructure and electrical properties of cryptomelane-type MnO_2 prepared by sol-gel method

Effect of doping Fe^{3+} and Cu^{2+} on the microstructure and electrical properties of cryptomelane-type MnO_2 prepared by sol-gel method

E Hastuti[1,*], W R Agustin[1] and I Yuliana[1]

[1]Department of Physics, Universitas Islam Negeri Maulana Malik Ibrahim Malang
Jl Gajayana 50 Malang, Indonesia

[*]E-mail : *erna@fis.uin-malang.ac.id*

Abstract. Manganese oxide (MnO_2) is an alternative metal oxide material that has potential as an energy storage application. In this study, the cryptomelane-type MnO_2 doped Fe^{3+} and Cu^{2+} were successfully prepared using the sol-gel method. Fumaric acid is added to the $KMnO_4$ in aqueous solution and modified with $FeCl_3.6H_2O$ and $CuCl_2.2H_2O$ to form different properties. Phase transformation and lattice parameters of the products were characterized using X-ray diffractometry (XRD). SEM observed the morphology of the sample, and electrical properties were tested using RCL meter. The results showed that adding Fe^{3+} and Cu^{2+} provided a higher value of conductivity and capacity of MnO_2.

1. Introduction

Manganese oxide is a transition metal oxide that studied as an electrode for supercapacitor applications. Manganese crystallize with various morphologies including the α, β, γ, ε, δ and R-polymorphs, which are naturally occurring minerals such as hollandite (2 x 2), pyrolusite (1 x 1), nsutite (1 x 1)/(1 x 2) with hexagonal structure, birnessite (1 x ∞), akhtenkite (dense stack), spinel (1 x 1), and ramsdellite (1 x 2) [1]. One of the most studied phases of manganese oxides is cryptomelane. Cryptomelane tunnels consist of 2 x 2 arrays of MnO_6 units and contain different interstitial cations Ba^{2+}, K^+, and Pb^{2+}, respectively [2].

The theoretical capacitance of manganese oxide reaches 1370 $F.gr^{-1}$ [3], but the electrochemical reversibility of the redox transition from manganese dioxide is usually low to apply, and pure manganese dioxide has an inadequate capacitive response. Despite this, manganese oxide is seen as potentially useful material for pseudocapacitor because of the theoretical capacitance it has, and environmentally friendly. Structural parameters, morphology, and conductivity are important in determining and optimizing the electrochemical properties of MnO_2.

Besides, various methods have been used to prepare MnO_2 nanostructures such as electrochemical deposition [4], coprecipitation [5], hydrothermal reactions [6], and sol-gel [7]. Of these methods, the sol-gel process has been very intriguing because of its unconventional approach. The gels were generated by redox reactions between alkali metal permanganates and fumaric acid [8]. Drying and calcination of the xerogels yielded the spinel phase, which was examined for their structural, morphology, and electrical characteristics. The sol-gel method requires simple equipment and can realize the chemical control at the molecular level and geometry control at the mesoscopic level. Thus the product has good chemical homogeneity, high purity and fine particles [9]. Another approach to improve the performance

of MnO_2 is by adding other metals such as Sn, Al, Cu, Mg [4], Cu [10], Fe [11], Al [12], Fe^{3+} [6], Co [13], V [14] and metal cations Ba^{2+}, K^+ [15].

In this study, MnO_2 was prepared from the sol-gel method and modified by doping Fe^{3+} and Cu^{2+} ions. The cryptomelane was obtained by calcining the xerogels from reactions between $KMnO_4$ with fumaric acid.

2. Methods

2.1. Synthesis of MnO_2

All chemical reagents were purchased in analytical grade and used without purification. Potassium permanganate ($KMnO_4$), Fumaric acid ($C_4H_4O_4$), $FeCl_3.6H_2O$, and $CuCl_2.2H_2O$ used as precursors. MnO_2 prepared by a redox reaction between $KMnO_4$ and fumaric acid. 20 mmol $KMnO_4$ dissolved in 200 ml distilled water, and 6.7 mmol fumaric acids were added to the solution. After stirring for 30 minutes at room temperature, the solution will form a brown-black gel. The gel is then allowed to stand for an hour. Then the sample is filtered and washed using distilled water and dried at 100 ^oC. Finally, xerogel was calcined at 450 ^oC for 2 hours. The synthesis of MnO_2 doped Fe^{3+} and Cu^{2+} followed the above procedure. $FeCl_3.6H_2O$ and $CuCl_2.2H_2O$ were used as dopant reagent of Fe^{3+} and Cu^{2+} in a concentration 5 and 10 (% mole).

2.2. Characterization of MnO_2

The crystal structure of the sample was studied by X-ray diffraction (XRD) technique using the Philips X-Pert using Cu-Kα radiation (λ=1.54060 Å). The microstructure and morphology of MnO_2 were characterized by scanning electron microscopy (SEM, Hitachi SU 3500). The electrical measurement used LCR meter (Hioki 3532-50, HiTester), conducted at room temperature. MnO_2 with different doping concentrations were mixed with PVDF (Polyvinylidene fluoride) binder in a ratio of 1:0.08 (wt.) in DMSO (Dimethyl sulfoxide) to form homogeneous electrode slurries. The slurry was dried to form electrode sheets. The working electrode coated with silver conductive paste. All the electrical measurements were carried out at 1.5 Volt in the frequency range 5 kHz-1MHz.

3. Results and Discussion

X-ray diffraction is used to determine the phase, crystal structure, and lattice parameters of MnO_2 doped Fe^{3+} and Cu^{2+}. Figure 1 represents the XRD patterns of the pristine, Fe^{3+}, and Cu^{2+}-doped samples. For all samples, pattern detected peak that indexed the I4/m tetragonal symmetry display the typical pattern of the cryptomelane-MnO_2 material (JCPDS 29-1020). The intense and sharp diffraction peaks appear at the pristine sample indicating the high crystallinity and purity. No peaks related to Cu and Fe compounds are observed. But, in samples with Fe^{3+} and Cu^{2+} doping, the diffraction intensities decrease, especially in the MnO_2 with doping Fe. The differences in peak broadening reveal that MnO_2 is a mixture of crystalized and amorphous. This structure is probably due to the doping elements (Fe^{3+} and Cu^{2+}) substituting Mn^{4+} and causing oxygen vacancies.

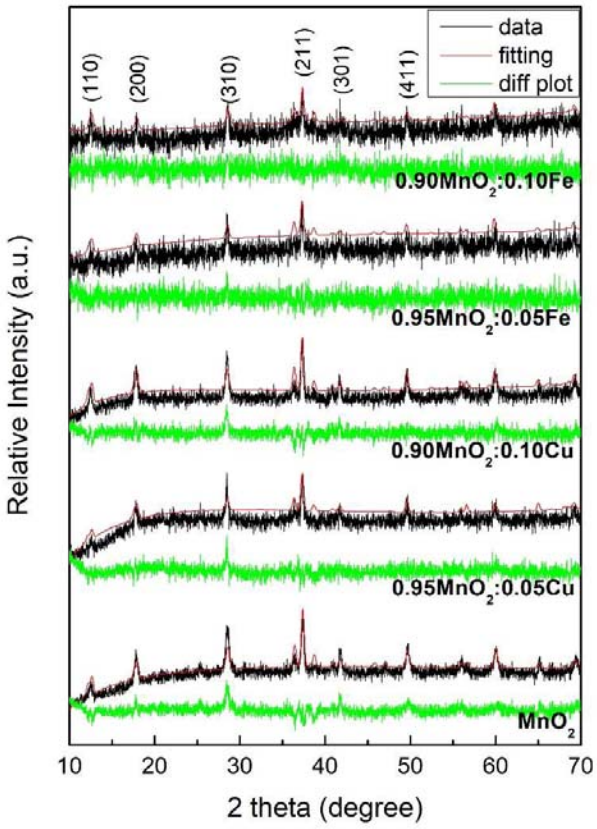

Figure 1. XRD patterns of the MnO_2.

Furthermore, to study the effect of doping on MnO_2, an analysis was performed using Rietveld refinement. The lattice parameter values a, b and c are shown in table 1.

Table 1. Lattice parameter determined by Rietveld refinement using Rietica software of samples.

Sample	Reliability Factor					Lattice parameters (Å)				V
	R_p	R_{wp}	R_B	R_{exp}	GOF	a	b	c	c/a	(Å)^3
MnO_2	5.66	7.47	7.34	5.34	1.95	9.8456	9.8456	2.8653	0.2910	277.750
MnO_2- Fe 5%	5.11	6.45	2.09	5.84	1.21	9.8701	9.8701	2.8738	0.2912	279.962
MnO_2- Fe 10%	4.54	5.69	1.13	5.31	1.15	9.8601	9.8601	2.8713	0.2912	279.152
MnO_2- Cu 5%	5.29	6.83	3.93	5.50	1.53	9.8609	9.8609	2.8682	0.2909	278.896
MnO_2-Cu 10%	5.65	7.16	5.39	5.82	1.51	9.8604	9.8604	2.8701	0.2911	279.053

Table 1 and figure 2 display variation of the lattice parameters and the change in the unit cell volume of cryptomelane-MnO_2 as a function of the doping concentration. As the ionic radius of dopant affects the lattice parameters of the α-MnO_2 phase, the lattice parameters and unit cell volume increase upon Cu^{2+} and Fe^{3+} doping slightly. But, the sample with doping 0.1 mole Fe^{3+}, the lattice parameter, and unit cell volume decrease. We can assume that the higher crystal radius of Fe^{3+} (0.785 Å) and Cu^{2+} (0.87 Å) replace Mn^{4+} (0.67 Å). However, the Fe^{3+} doping concentration of 0.1 (mole), the number of vacancies increased, thereby reducing the lattice parameter.

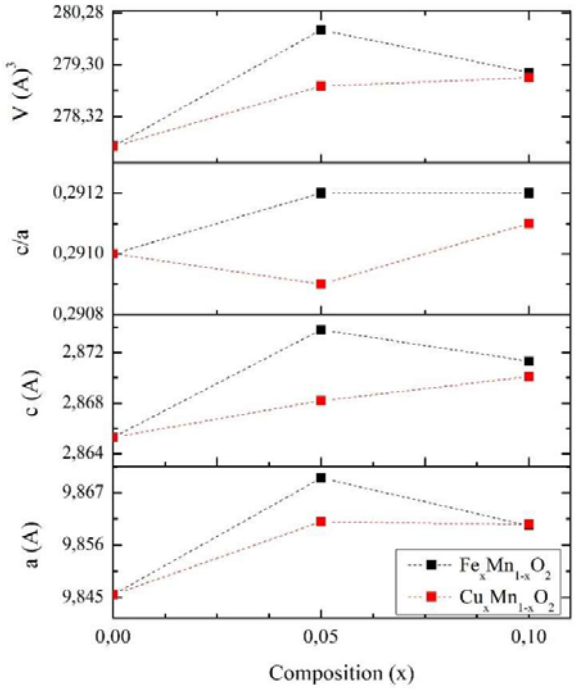

Figure 2. Lattice parameters and unit cell volume of MnO_2.

The morphologies of pristine and Fe^{3+}/Cu^{2+}-doped MnO_2 were characterized by scanning electron microscopy analysis, and the image is presented in figure 3. It can be seen that pristine and doped Cu^{2+} (Figure 3 (a, c) are composed of irregular spherical particles. The approximate size of particles in the range of 20-60 nm is interconnected and attributed to agglomeration. However, when MnO_2 is doped with Fe^{3+} (Figure 3(b)), morphology shows more agglomeration and amorphous surface. This morphology is following the XRD pattern in Figure 1.

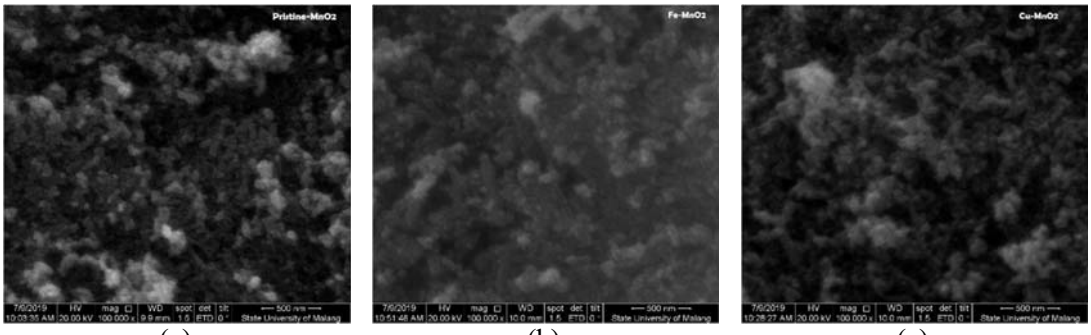

(a) (b) (c)

Figure 3. SEM image of MnO_2: (a) pristine; (b) Fe^{3+}-MnO_2; (c) Cu^{2+}-MnO_2.

Figure 4 shows the crystal structure of the studied sample, constructed by double chains of octahedron MnO_6 which are linked at the corner to form (2x2) tunnels. In the cryptomelane phase, K^+ ions occupy the (2x2) tunnels. Doping Fe^{3+} and Cu^{2+} substituting Mn^{4+} while oxygen vacancy can be found in the nearby of ion.

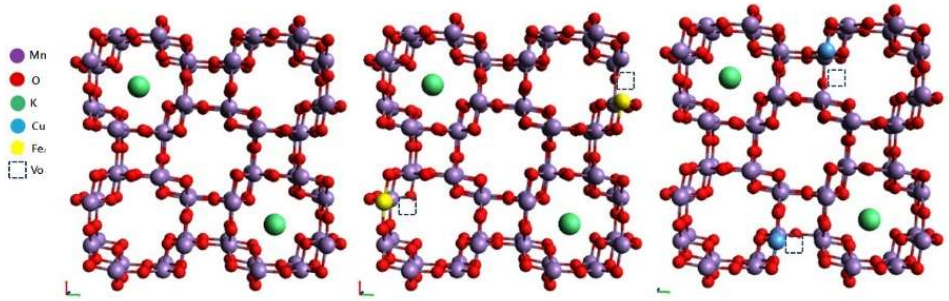

Figure 4. Crystal structure of Cryptomelane-MnO_2, possible substitution and defect.

The electrical performance of these doped-MnO_2 was investigated by RCL meter measurement. Figure 5 shows the electrical conductivity as a function of frequency for cryptomelane-type MnO_2 with different Fe^{3+} and Cu^{2+} doping. The results indicate the typical behavior for semiconducting material that obeys the power law [8]. The electronic conductivity of MnO_2 is $\approx 10^{-6}$ S.m^{-1} at room temperature [1]. Sample with doping Fe^{3+} and Cu^{2+} increase the electrical conductivity up to $\sim 10^{-3}$ S.m^{-1} at high frequency. It correlated with the XRD results that Fe^{3+} and Cu^{2+} replace Mn^{4+} in the cryptomelane structure, which can be compensated by the creation of oxygen vacancies, which results in structural distortion, especially at MnO_2 doped Fe^{3+}. These vacancies contribute to the increase in the conductivity of the doped samples.

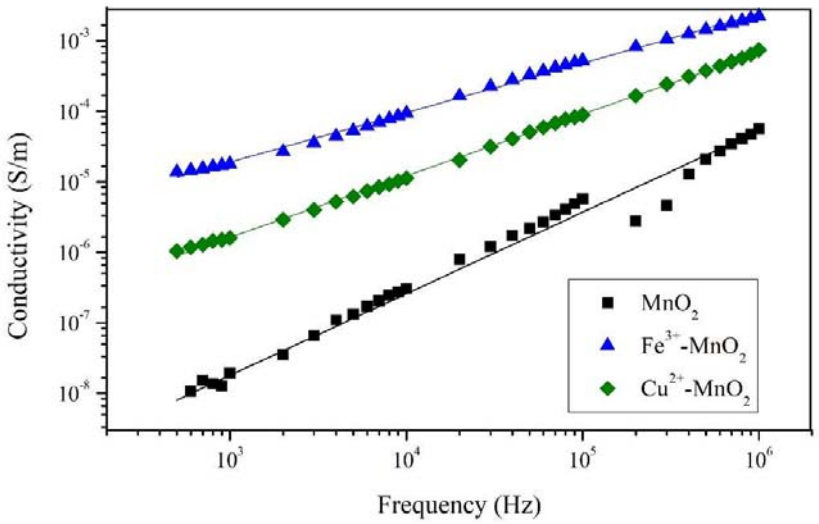

Figure 5. Conductivity of MnO_2.

Moreover, an increase in the areal capacitance was observed in the presence of dopants and compared with pristine α-MnO_2 material. The addition of dopant ions increases the amount of polarized charge. This polarization charge creates an electric field through the Maxwell-Gauss equation, which will attract mobile charges of opposite sign, resulting in the same situation as the impurity-based doping: a mobile charge linked to a polarization charge in one case, related to an ionized dopant in the other case [16].

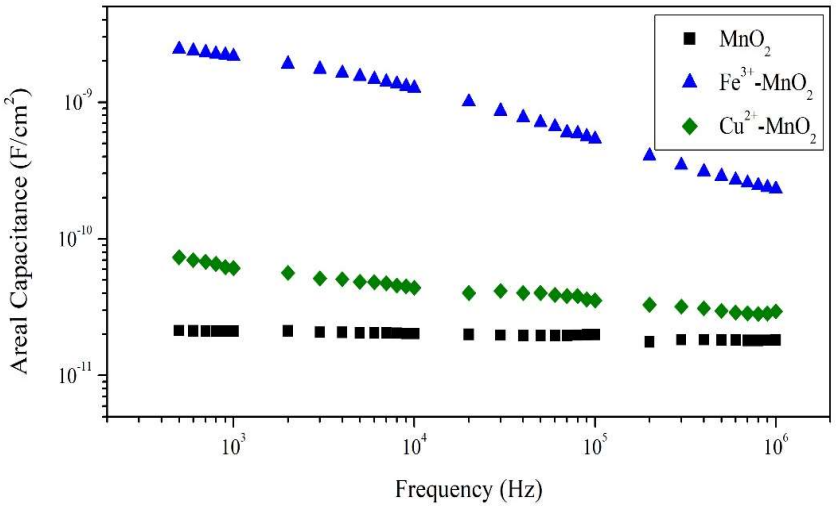

Figure 6. Plots of the areal capacitance of MnO_2.

The MnO_2-doped Fe^{3+} in fig 6 shows higher areal capacitance over that of pristine and doping Cu^{2+}. The smaller particle size and lower crystallinity of Fe^{3+}-MnO_2 (Figure 1,2) facilitate the polarization processes within the material and increasing the capacitance. In addition, the radius of the Fe^{3+} ion which is smaller than the Cu^{2+} ion has an important influence on the value of the capacitance [17].

4. Conclusion

Transition metal (Fe^{3+}, Cu^{2+}) doped cryptomelane-type manganese oxides have been successfully synthesized by the sol-gel method. The XRD data suggested that materials were crystalline without impurities. Adding Fe^{3+} and Cu^{2+} did not affect the crystal structure (α-MnO_2) but changed the lattice parameters and morphology. The reaction between metal ions and Mn ions occurs during the process. Fe^{3+} and Cu^{2+} replace the Mn^{4+} and causing oxygen vacancies. Because of the substitution and differences in ionic radii, lattice parameters increase with doping. But at the Fe^{3+} doping concentration of 0.1 (mole), the number of vacancies increased and reduced the lattice parameter. This result is associated with lower crystallinity and smaller particle size. In addition, this sample also exhibits excellent electrical properties. The results of the conductivity indicate that doping can increase ion mobility and charge transfer which improves the capacitance performance of the material.

References

[1] Christian Julien and Alain Mauger 2017 *Nanomaterials* **7** 396
[2] Ching S, Welch E J, Hughes S M, Bahadoor A B F and Suib S L 2002 *Chem. Mater.* **14** 1292–9
[3] Hu J, Qian F, Song G, Li W and Wang L 2016 *Nanoscale Res. Lett.* **11**
[4] Hashem A M, Abdel-Latif A M, Abuzeid H M, Abbas H M, Ehrenberg H, Farag R S, Mauger A and Julien C M 2011 *J. Alloys Compd.* **509** 9669–74
[5] Poonguzhali R, Gobi R, Shanmugam N, Senthil Kumar A, Viruthagiri G and Kannadasan N 2015 *Mater. Lett.* **157** 116–22
[6] Wang J-G, Yang Y, Huang Z-H and Kang F 2012 *Mater. Chem. Phys.* **133** 437–44
[7] Tang W, Shan X, Li S, Liu H, Wu X and Chen Y 2014 *Mater. Lett.* **132** 317–21
[8] Hashem A M A, Mohamed H A, Bahloul A, Eid A E and Julien C M 2008 *Ionics* **14** 7–14
[9] Liu T-T, Shao G-J, Ji M-T and Ma Z-P 2013 *Asian J. Chem.* **25** 7065–70
[10] Zhao S, Liu T, Javed M S, Zeng W, Hussain S, Zhang Y and Peng X 2016 *Electrochimica Acta* **191** 716–23
[11] Dubal D P and Lokhande C D 2013 *Ceram. Int.* **39** 415–23

[12] Hu Z, Xiao X, Chen C, Li T, Huang L, Zhang C, Su J, Miao L, Jiang J, Zhang Y and Zhou J 2015 *Nano Energy* **11** 226–34
[13] Tang C-L, Wei X, Jiang Y-M, Wu X-Y, Han L, Wang K-X and Chen J-S 2015 *J. Phys. Chem. C* **119** 8465–71
[14] Alfaruqi M H, Islam S, Mathew V, Song J, Kim S, Tung D P, Jo J, Kim S, Baboo J P, Xiu Z and Kim J 2017 *Appl. Surf. Sci.* **404** 435–42
[15] Zhai D, Li B, Xu C, Du H, He Y, Wei C and Kang F 2011 *J. Power Sources* **196** 7860–7
[16] Jamaux J 2014 *Polarization-induced doping and its application to light-emitting diodes* (Quebec: McGill University)
[17] Mariappan C R, Heins T P and Roling B 2010 *Solid State Ion.* **181** 859–63